doi:10.1016/j.jmb.2008.10.055 J. Mol. Biol. (2009) 385, 889–901

JMB

Available online at www.sciencedirect.com

ScienceDirect

ELSEVIER

Structural Aspects of the Distinct Biochemical Properties of Glutaredoxin 1 and Glutaredoxin 2 from *Saccharomyces cerevisiae*

Karen Fulan Discola[1,2], Marcos Antonio de Oliveira[2,3], José Renato Rosa Cussiol[2], Gisele Monteiro[2], José Antonio Bárcena[4], Pablo Porras[4], C. Alicia Padilla[4], Beatriz Gomes Guimarães[5] and Luis Eduardo Soares Netto[2]*

[1]*Departamento de Bioquímica, Instituto de Biologia, Universidade Estadual de Campinas, 13083-970 Campinas, Brazil*

[2]*Departamento de Genética e Biologia Evolutiva, Instituto de Biociências, Universidade de São Paulo, 05508-900 São Paulo, Brazil*

[3]*Departamento de Biologia, Universidade Estadual Paulista, 11330-900 São Vicente, Brazil*

[4]*Departamento de Bioquímica y Biología Molecular, Universidad de Córdoba, 14071 Córdoba, Spain*

[5]*Laboratório Nacional de Luz Síncrotron, Campinas, Brazil*

Received 27 May 2008; received in revised form 6 October 2008; accepted 15 October 2008
Available online 28 October 2008

Edited by R. Huber

Glutaredoxins (Grxs) are small (9–12 kDa) heat-stable proteins that are ubiquitously distributed. In *Saccharomyces cerevisiae*, seven Grx enzymes have been identified. Two of them (yGrx1 and yGrx2) are dithiolic, possessing a conserved Cys-Pro-Tyr-Cys motif. Here, we show that yGrx2 has a specific activity 15 times higher than that of yGrx1, although these two oxidoreductases share 64% identity and 85% similarity with respect to their amino acid sequences. Further characterization of the enzymatic activities through two-substrate kinetics analysis revealed that yGrx2 possesses a lower K_M for glutathione and a higher turnover than yGrx1. To better comprehend these biochemical differences, the pK_a of the N-terminal active-site cysteines (Cys27) of these two proteins and of the yGrx2-C30S mutant were determined. Since the pK_a values of the yGrx1 and yGrx2 Cys27 residues are very similar, these parameters cannot account for the difference observed between their specific activities. Therefore, crystal structures of yGrx2 in the oxidized form and with a glutathionyl mixed disulfide were determined at resolutions of 2.05 and 1.91 Å, respectively. Comparisons of yGrx2 structures with the recently determined structures of yGrx1 provided insights into their remarkable functional divergence. We hypothesize that the substitutions of Ser23 and Gln52 in yGrx1 by Ala23 and Glu52 in yGrx2 modify the capability of the active-site C-terminal cysteine to attack the mixed disulfide between the N-terminal active-site cysteine and the glutathione molecule. Mutagenesis studies supported this hypothesis. The observed structural and functional differences between yGrx1 and yGrx2 may reflect variations in substrate specificity.

Keywords: glutaredoxin; *Saccharomyces cerevisiae*; glutathione; disulfide; X-ray structure

**Corresponding author.* E-mail address: nettoles@ib.usp.br.
Present address: Synchrotron SOLEIL, Saint-Aubin, France.

Abbreviations used: Grx, glutaredoxin; GR, glutathione reductase; GSH, reduced glutathione; GSSG, oxidized glutathione, glutathione disulfide; HED, β-hydroxyethyl disulfide; β-ME-SG, glutathionylated β-mercaptoethanol; *t*-BOOH, *tert*-butyl-hydroperoxide; yGrx1, glutaredoxin 1 from yeast; $yGrx1_{GS}$, yeast Grx1-C30S mutant glutathionylated; $yGrx1_{red}$, yeast Grx1 reduced; yGrx2, glutaredoxin 2 from yeast; $yGrx2_{GS}$, yeast Grx2-C30S mutant glutathionylated; $yGrx2_{ox}$, yeast Grx2 oxidized; BSA, bovine serum albumin; EDTA, ethylenediaminetetraacetic acid.

Introduction

Glutaredoxins (Grxs) are small, heat-stable oxidoreductases with conserved cysteine residues present in CXXC motifs.[1] These oxidoreductases are reduced by glutathione (GSH), producing glutathione disulfide (GSSG) that is then reduced by NADPH in a reaction catalyzed by glutathione reductase (GR).[1] Grxs were first discovered in *Escherichia coli* as dithiol, GSH-dependent hydrogen donors for ribonucleotide reductase in a mutant lacking thioredoxin.[2] Later, it was described that Grxs can also reduce mixed disulfides between proteins or low molecular weight thiols and GSH in reactions that require only their N-terminal active-site cysteine.[3–5] It is important to note that the reduction of glutathionylated substrates through the monothiol mechanism seems to be the major activity of Grxs; all dithiol Grxs described so far catalyze these reactions, but not all dithiol Grxs catalyze the reduction of protein disulfides by the dithiol mechanism.[6] Therefore, Grxs are receiving increasing attention in redox regulation processes due to their ability to catalyze the reduction of disulfides.[7]

In the monothiol mechanism, Grxs specifically interact with the GSH moiety of the protein-SG mixed disulfide target, using only the N-terminal cysteine of the CXXC motif (Fig. 1, reaction a).[5,9] A covalent Grx-SG mixed intermediate is formed and the target protein is released in its reduced form. Then, a second molecule of GSH reduces the Grx-SG mixed intermediate, generating reduced Grx and GSSG (Fig. 1, reaction b).[10] GSSG is then reduced by GR at the expense of NADPH.

The reduction of the Grx-SG mixed disulfide by the second GSH molecule (Fig. 1, reaction b) is the rate-determining step of the overall process.[8] If the reduction of the Grx-SG by an external nucleophile such as GSH is favored, the reaction tends to proceed by the monothiol mechanism. However, if the nucleophilic attack of the C-terminal cysteine on the Grx-SG is favored, a side reaction can occur and produce oxidized Grx with an intramolecular disulfide bond (Fig. 1, reaction c). In this case, the reaction proceeds through the dithiol mechanism, and the disulfide bond of Grx is reduced by two GSH molecules.[11,12]

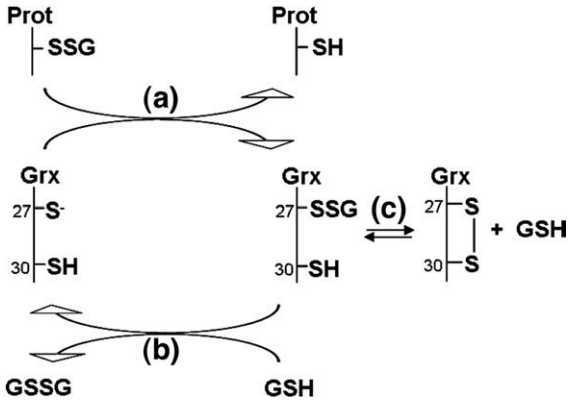

Fig. 1. Scheme of Grx monothiol mechanism. (a) The N-terminal cysteine of the Grx active site interacts with the GSH moiety of the protein-SG mixed disulfide target, then a covalent Grx-SG mixed intermediate is formed and the target protein is released in its reduced form. (b) A second molecule of GSH reduces the Grx-SG mixed intermediate, generating reduced Grx and glutathione disulfide (GSSG). (c) The oxidized form of Grx with an intramolecular disulfide bond can be formed by the nucleophilic attack of Cys30 and is reduced back by two GSH molecules. Adapted from Srinivasan *et al.*[8]

Another common feature of Grxs is that the pK_a of their N-terminal active-site cysteine thiol is generally very low (around 3.0 to 4.0). Therefore, most of these cysteine residues are deprotonated at physiological pH, whereas the C-terminal active-site cysteine is usually protonated.[12–14] The thiolate form of the N-terminal cysteine of Grx appears to contribute to its catalytic activity because it is a good leaving group (Fig. 1, reaction b) rather than a good nucleophile (Fig. 1, reaction a), which is in line with the observation that reaction b is the rate-limiting step.[8,12]

In *Saccharomyces cerevisiae*, seven Grx genes have been identified (*GRX1–7*). Glutaredoxin 1 and 2 from yeast (yGrx1 and yGrx2) are dithiolic Grxs, which contain the conserved CPYC motif in their active sites.[15] yGrx2 is present in two molecular weight isoforms (11,900 and 15,900), each synthesized by one of two in-frame translation initiation start sites.[16] The cytosolic isoform is synthesized from the second AUG and lacks an N-terminal extension, while the long isoform that carries a mitochondrial targeting presequence is translated from the first AUG.[17] The latter is translocated to the mitochondria where it is either processed by the mitochondrial processing peptidase to a short soluble isoform that localizes to the matrix or left unprocessed and retained in the outer mitochondrial membrane.[17] yGrx3, yGrx4 and yGrx5 are monothiol isoforms that contain the motif CGFS in their active sites.[18] yGrx3 and yGrx4 are required for Aft1 iron regulation in the nucleus, whereas yGrx5 is thought to be involved in iron–sulfur cluster metabolism and assembly.[19,20] Recently, two other monothiolic enzymes, yGrx6 and yGrx7, were described in *S. cerevisiae*.[21]

The current work is focused on the two dithiolic enzymes, yGrx1 and the short isoform of yGrx2. These proteins are highly similar (64% identity and 85% similarity), although single deletions of their genes have rendered yeast mutants with distinct phenotypes.[15] Δ*GRX1* is sensitive to oxidative stress caused by superoxide anion, whereas Δ*GRX2* is sensitive to stress induced by hydrogen peroxide.[15] Furthermore, studies with yeast knockouts have indicated that yGrx2 accounts for most of the GSH-dependent oxidoreductase activity in the cell.[15] Since yGrx1 and yGrx2 expression levels are similar,[15] the exhibited phenotypes in knockout strains could reflect that yGrx2 is a more efficient enzyme than yGrx1.

We compared recombinant dithiolic Grxs from yeast and observed that the specific activity of yGrx2

was 15 times higher than that of yGrx1 in the standard β-hydroxyethyl disulfide (HED) assay, despite their high amino acid sequence similarity. Bisubstrate kinetics analysis indicated that both K_M toward GSH and turnover rate account for this enzymatic difference. In an attempt to better understand the functional differences between yGrx1 and yGrx2, we elucidated the crystallographic structure of yGrx2 in the oxidized state and of the yGrx2-C30S mutant in complex with GSH through a mixed disulfide. Comparisons between these structures and those of yGrx1[22] revealed that residues near the active-site region could be directly implicated in the functional differences of yGrx1 and yGrx2. Mutagenesis studies supported this hypothesis.

Results and Discussion

yGrx2 is more active as an oxidoreductase than yGrx1

Yeast cell-free extracts from Δ*GRX2* but not from Δ*GRX1* lose most of their GSH-dependent oxidoreductase activity,[15] indicating that yGrx2 accounts for the majority of this enzymatic activity. Based on this observation, we measured the specific activities of pure recombinant yeast dithiolic Grxs, using the standard assay of reduction of the mixed disulfide formed between HED and GSH (glutathionylated β-mercaptoethanol, β-ME-SG).[23] yGrx2 was approximately 15 times more active than yGrx1 (Table 1, Supplementary Data), although they share a high level of sequence similarity (Fig. 2a).

To eliminate any artifacts due to metal contamination, which could result from leaching of nickel during affinity chromatography, we compared the activity results of yGrx1 and yGrx2 purified with cobalt-affinity chromatography. Although cobalt binds more strongly to a Talon affinity column (Clontech) than nickel to a Hi-Trap affinity column (GE Healthcare), the specific activities were essentially the same. Furthermore, we also removed the N-terminal his-tag from the yGrx1 and yGrx2 recombinant proteins, but their oxidoreductase activities remained the same. Therefore, yGrx2 is intrinsically more active than yGrx1, which explains results of previous studies on yeast knockout strains.[15]

Two-substrate kinetics for yGrx1 and yGrx2

In order to better characterize the activity of yeast dithiol Grxs, we varied the concentration of HED at different concentrations of GSH and determined the apparent K_M and k_{cat} of yGrx1 and yGrx2 for β-ME-SG (Table 2).[21,26] β-ME-SG was formed during a 3-min preincubation and the reactions were started with the addition of Grx. We confirmed in separate experiments that the GR concentration used was not rate limiting (data not shown). The apparent K_M and V_{max} values were determined by non-linear regression of Michaelis–Menten plots (see Supplementary Data). yGrx1 presented higher affinity (lower apparent K_M values) for β-ME-SG than yGrx2, but a lower turnover number (lower k_{cat} values) than yGrx2 (Table 2). These parameters are related to the formation of the Grx-SG mixed disulfide (Fig. 1, reaction a). As a consequence, the catalytic efficiency (k_{cat}/K_M in M^{-1} s^{-1}) of yGrx1 is approximately five times lower compared with yGrx2.

Kinetic data linearization by Lineweaver–Burk resulted in intersecting lines on double-reciprocal plots (data not shown), which indicates a sequential mechanism for both yGrx1 and yGrx2. Similar patterns were obtained for yGrx7 and human Grx from red blood cells in the HED assay, which confirm that the β-ME-SG formation in the preincubation reaction is nonenzymatic.[21,26]

We built secondary plots with the reciprocal values of V_{max}^{app} *versus* the reciprocal of GSH concentrations to obtain the "true" kinetics parameters (Fig. 3a and b).[27] yGrx2 has a lower K_M for GSH than yGrx1 and a higher turnover number, resulting in a

Table 1. Values of specific activity* and pK_a of Cys27 for yGrx1, yGrx2, and the mutants yGrx1-C30S, yGrx1-S23A, yGrx1-S23A-Q52E, yGrx2-C30S, yGrx2-A23S and yGrx2-A23S-E52Q

Protein	Specific activity (μmol min^{-1} mg^{-1})	pK_a Cys27[a]	
		Monobromobimane alkylation	Iodoacetamide inactivation
Grx1	8.2±0.3	3.2±0.2	4.0±0.2
Grx1-C30S	38.7±0.5	N.D.	N.D.
Grx1-S23A	27.8±0.5	N.D.	N.D.
Grx1-S23A-Q52E	24.5±0.4	N.D.	N.D.
Grx2	125±7	3.1±0.2	3.5±0.2
Grx2-C30S	38±1	N.D.	3.2±0.2
Grx2-A23S	74±5	N.D.	N.D.
Grx2-A23S-E52Q	54±2	N.D.	N.D.

* The reaction mixture for the determination of specific activities contained 100 mM Tris–HCl pH 7.4, 6 μg/ml GR, 1 mM GSH, 0.7 mM HED, 0.1 mg/ml BSA, 0.2 mM NADPH and 2 mM EDTA. For more details, see Materials and Methods. N.D., not determined.

[a] pK_a values were obtained from inflection points in sigmoidal dose–response curves with Hill slope equal to 1 as described in Materials and Methods and Supplementary Material.

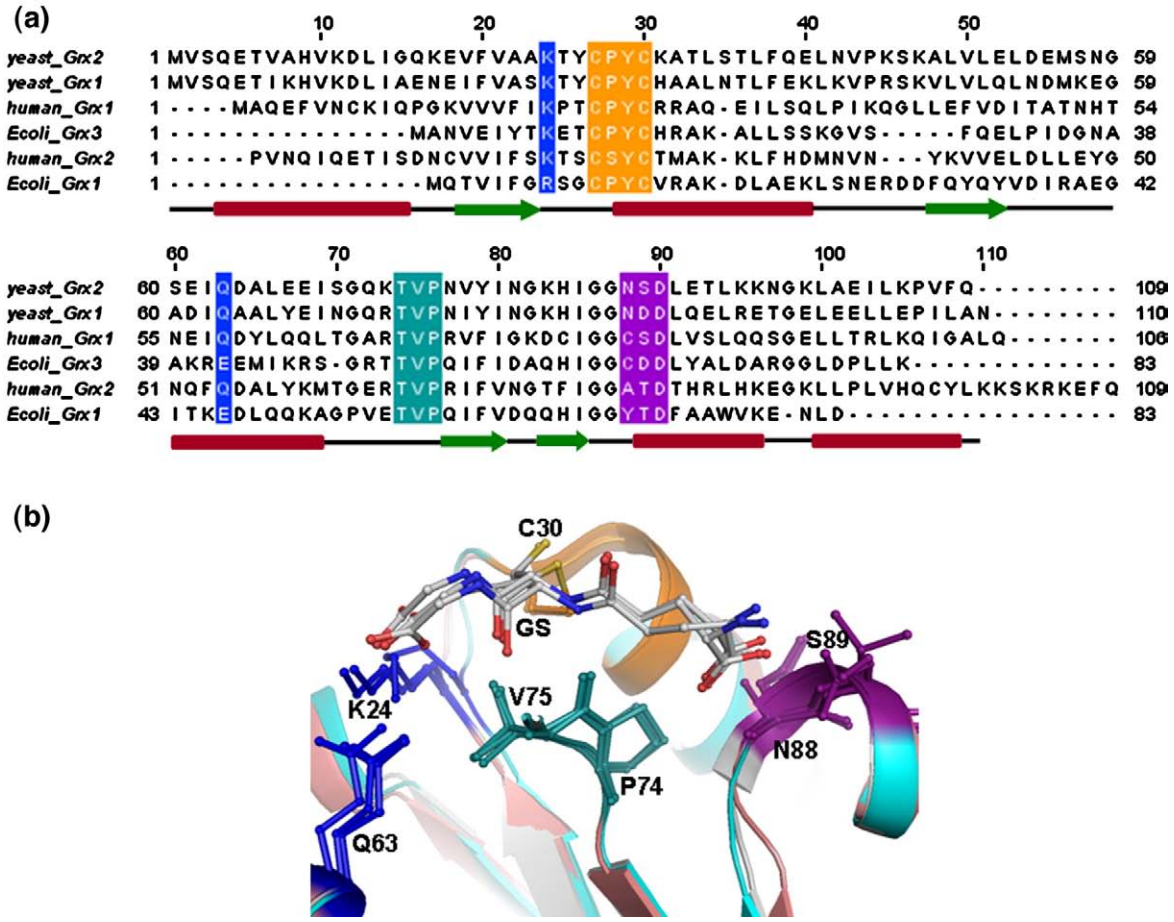

Fig. 2. Alignment of Grxs with glutathionylated structures. (a) Sequences were aligned using ClustalW[24] and the alignment representation was produced with Jalview.[25] The active-site residues of Grxs are highlighted with an orange rectangle and residues within the blue rectangles are involved in interactions with the Gly residue from GSH. The green rectangle indicates residues that form the TVP motif involved in interactions with the Cys residue from GSH, and within the violet rectangle are the residues participating in interactions with the GSH γ-Glu residue. The secondary-structure elements of yGrx2 are indicated at the bottom of the figure (arrows representing β-sheets and cylinders for α-helices). (b) Structural superposition of yGrx2 (cyan), yGrx1 (gray) and human Grx2 (pink) glutathionylated structures. The residues involved in interactions with the GSH moiety are identified with the sequence number of yGrx2, and residues highlighted in (a) are shown in the same colours.

catalytic efficiency 2 orders of magnitude higher than that of yGrx1 (Table 3). Since these parameters are related to the rate-limiting step (Fig. 1, reaction b) of the overall monothiol mechanism, both the lower K_M for GSH and higher turnover number are responsible for the high specific activity of yGrx2 (Table 3).

Properties of the yGrx1-C30S and yGrx2-C30S mutants

As previously described, the substitution of the C-terminal active-site cysteine by a serine residue in dithiolic Grxs does not abolish the GSH-dependent oxidoreductase activity in the HED assay because it

Table 2. Apparent kinetic constants for the reduction of the mixed disulfide formed between GSH and HED by yGrx1 and yGrx2, determined from Michaelis–Menten plots

yGrx1			yGrx2		
[GSH] (mM)	K_M^{app} (mM)	k_{cat}^{app} (s^{-1})	[GSH] (mM)	K_M^{app} (mM)	k_{cat} (s^{-1})
0.5	0.12	1.3	0.5	0.9	47
1.0	0.12	2.2	1.0	0.7	66
1.5	0.14	3.5	1.5	0.6	85
2.0	0.13	4.2			

The reaction mixture contained 100 mM Tris–HCl, pH 7.4, 6 μg/ml GR, 0.1 mg/ml BSA, 0.2 mM NADPH and 2 mM EDTA. The concentration of HED was varied from 0.03 to 2.2 mM at fixed concentrations of GSH, and the reactions were started by the addition of 500 or 50 nM of yGrx1 or yGrx2, respectively.

proceeds via the monothiol mechanism.[5,13,28] The yGrx1-C30S mutant presented higher specific activity than wild-type yGrx1, similarly to the mutants for the C-terminal active-site cysteine of human Grx1 and Grx2 and pig Grx (Table 1).[13,28,29] Nevertheless, the specific activity of yGrx2-C30S decreased to 38±2 μmol min^{-1} mg^{-1}, which corresponds to 30% of the wild-type yGrx2 activity (Table 1). This observation is very consistent with data previously reported for C14S mutants of Grx1 and Grx3 from *E. coli*.[5,11]

As mentioned before, it was described for human Grx1 that the overall reaction rate in the HED assay is determined by the rate of Grx-SG intermediate reduction.[8] The occurrence of the side reaction (Fig. 1, reaction c), which results in the formation of the intramolecular disulfide bond, is implicated in a decrease in the reaction rate, probably because part of the enzyme and GSH are involved in a nonproductive exchange reaction.[28] The substitution of the C-terminal active-site cysteine by a serine residue in dithiolic Grxs eliminates the possibility of this side reaction and in principle should increase the reaction rate. This was the case for yGrx1-C30S, pig Grx and the human Grx1 and Grx2 mutants.[13,28,29]

However, for yGrx2-C30S and *E. coli* Grx1 and Grx3, the same mutation causes a decrease in specific activity.[5,11] The reasons for this effect are not clear but might be related to differential structural features among different Grx isoforms. Future studies are necessary in order to better understand the particularities of these enzymes.

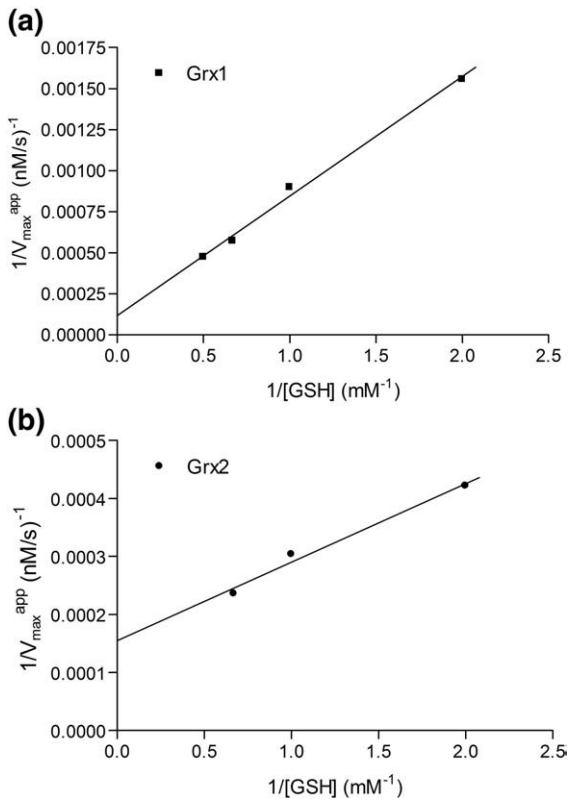

Fig. 3. Secondary plots (reciprocal values of V_{max}^{app} *versus* the reciprocal of GSH concentration) used for the determination of the kinetic constants of yGrx1 (a) and yGrx2 (b) for GSH.

Table 3. Kinetic constants for the reduction of the mixed disulfide formed between GSH and HED by yGrx1 and yGrx2, obtained with the secondary plots of $1/V_{max}^{app}$ *versus* 1/[GSH]

	GSH		
Protein	K_M (mM)	k_{cat} (s^{-1})	k_{cat}/K_M $(M.s)^{-1}$
Grx1	6.2	17.1	2.75×10^3
Grx2	0.9	129	1.43×10^5

The pK_a of reactive cysteines cannot explain the difference between the oxidoreductase activities of the dithiolic yGrxs

In the previous sections, it was demonstrated that yGrx2 possesses higher activity than yGrx1, which is related to both a lower K_M for GSH and higher turnover (k_{cat}). It is well known that the N-terminal active-site cysteine residue of Grxs possesses a very low pK_a value and that this feature is important for catalysis.[8,12–14] Therefore, a significant difference in the pK_a values of yGrx1 and yGrx2 might explain the variation in the reactivities between these two enzymes.

The pK_a relative to the thiol group of the N-terminal active-site cysteine (Cys27) of both yGrx2 and yGrx1 were determined by two independent methods (Table 1, Fig. 4). The values obtained by iodoacetamide inactivation are very similar to those previously determined for yGrx2 and human Grx1 using the same approach.[12,14] The substitution of the C-terminal cysteine to a serine in the yGrx2-C30S mutant resulted in a slight decrease (not significant) in the pK_a value of Cys27 (Table 1, Fig. 4a). Furthermore, analysis by specific thiolate monobromobimane alkylation (which generates a fluorescent adduct)[30] indicated that the pK_a values of Cys27 from yGrx1 and yGrx2 are even more similar if not identical (Table 1, Fig. 4b). In the case of yGrx1, although the pK_a values for yGrx1 Cys27 determined by the independent approaches presented some divergence (Table 1), both of them indicated that the corresponding sulfhydryl moiety should be present mostly as thiolate under physiological conditions.

Thiol–disulfide exchange reactions are expected to proceed as S_N2-type, in which the rate is dependent on the basicity (pK_as) of the nucleophile and the leaving groups[31,32] and the reactive specie is the ionized thiolate.[33] For a thiol–disulfide exchange reaction where the thiolate anion (SR_{nuc}) attacks one of the two sulfur atoms of the disulfide bond, the central sulfur (SR_c) will have the higher pK_a value.[8,12] As described by the following reaction,

$$SR_{nuc} + SR_{lg}SR_c \rightarrow SR_{nuc}SR_c + SR_{lg}$$

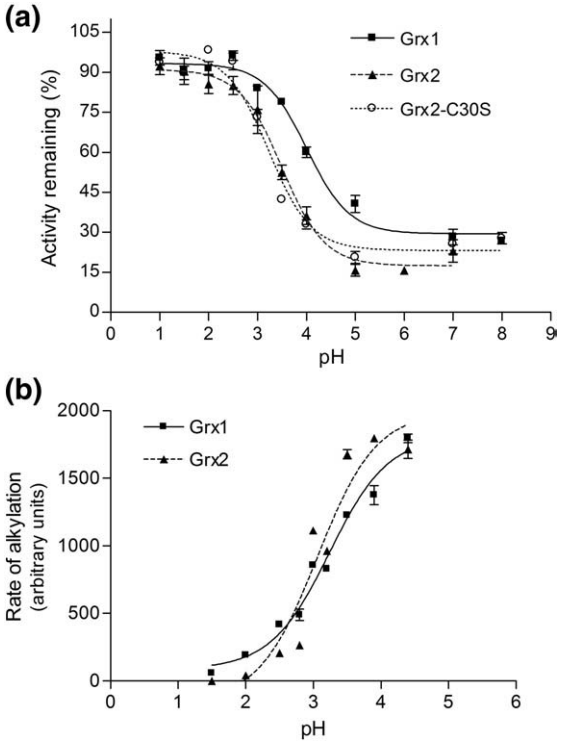

Fig. 4. Determination of pK_a values for reactive cysteines. (a) Iodoacetamide inactivation. yGrx1 (filled squares), yGrx2 (filled triangles) and yGrx2-C30S (open circles). The enzymes (250 nM yGrx1, 20 nM yGrx2, or 100 nM yGrx2-C30S) were incubated with 300 μM iodoacetamide at different pH values for 3 min at room temperature and then assayed using the standard assay for Grxs after a 100-fold dilution. The percentage of remaining activity at each pH was determined by comparing the activity of the enzyme incubated with and without iodoacetamide. All buffers were used at a concentration of 10 mM and ionic strength was adjusted with the addition of 0.5 M NaCl. (b) Monobromobimane alkylation. yGrx1 (filled squares) and yGrx2 (filled triangles). The prereduced yGrx1 and yGrx2 enzymes (10 μM) were alkylated with 2 μM of monobromobimane at different pH values, as described in Materials and Methods.

the lower the pK_a of the leaving sulfur (SR_{lg}), the faster the rate will be, according to the Brønsted equation: $\log k = c + \beta_{nuc} pK_{a(nuc)} + \beta_c pK_{a(c)} + \beta_{lg} pK_{a(lg)}$, where β_{nuc}, β_c and β_{lg} are the Brønsted base coefficients for the nucleophile, central group and leaving group, respectively.[8,12] Accordingly, for a given homologous set of thiol–disulfide exchange reactions, the second-order rate constant increases by a factor of four for each unit decrease in the pK_a of the leaving group ($\Delta k = 4\Delta^{pKa}$).[31,32] Assuming that GSH-mediated reduction of the Grx-SG intermediate is the rate-limiting step in the HED assay,[8] the difference in the pK_a values of yGrx1 and yGrx2 Cys27 residues would result in an increase of the rate constant of yGrx2 by 2.0-fold relative to that of yGrx1 when the results from iodoacetamide inactivation are considered, and an increase of 1.15-fold when the results from monobromobimane alkylation are considered (Table 1). However, the difference observed in the enzymatic activities is much higher than expected due to the difference in the pK_a values, suggesting the involvement of other factors, possibly structural features. Although the Brønsted equation applies quite well to low molecular weight thiols,[32] some deviation occurs in proteins,[12] further indicating that structural features besides pK_a values are important in controlling thiol–disulfide exchange rates.

It is important to mention that in this work we have assumed that the rate-limiting reaction in the HED assay for yGrxs is the reduction of the Grx-SG mixed disulfide intermediate, as described for human Grx1.[8] This is because yGrx2 activity presented a pH dependence similar to that of human Grx1, with a pH optimum value near 9.0.[14] Also, Cys27 from yGrx1 and yGrx2 presented pK_a values similar to that of human Grx1, suggesting that the thiolate pK_a of the second substrate (GSH) is involved in the rate-determining step.[8,26] Therefore, when all the information are taken together, pK_a values for yGrx1 and yGrx2 Cys27 should not be an important factor in the control of the overall reaction rate.

Crystal structures of yGrx2

Since the pK_a values of the reactive cysteines did not correlate with their intrinsic activities, we decided to compare the structural features of yGrx1 and yGrx2. The crystal structures of yGrx1 in the reduced and glutathionylated forms (named here as $yGrx1_{red}$ and $yGrx1_{GS}$, respectively) were recently reported,[22] and to perform comparisons, we crystallized yGrx2 and solved its structure in two different forms.

Before crystallization, yGrx2 was subjected to treatments with oxidizing [*tert*-butyl-hydroperoxide (*t*-BOOH), diamide and hydrogen peroxide] and reducing (DTT and GSH) agents in an attempt to obtain its structure in different oxidation states. The first structure was solved and refined at 2.05 Å resolution, corresponding to yGrx2 pretreated with *t*-BOOH (named herein as $yGrx2_{ox}$). The $yGrx2_{ox}$ structure was used as a search model to solve the other structures of yGrx2 under different treatments. After structure solving and refinement of all data sets, we observed that in all cases (even in proteins treated with reductants), the two cysteines in the active site were oxidized, forming an intramolecular disulfide bond. The alignment of these structures showed that they were identical, and electron density map analyses indicate that no oxidation of any other residue, except the active-site cysteines, was observed, not even in the structure of yGrx2 pretreated with *t*-BOOH. We then performed analysis on the oxidized structure obtained from the data set that presented the best resolution and statistics (Table 4). Other attempts were made to obtain yGrx2 structure in the reduced form, but all of them failed.

In another attempt to obtain the reduced structure of yGrx2, we constructed the yGrx2-C30S mutant, which was also used to obtain the yGrx2 structure

Table 4. Diffraction and refinement statistics of oxidized and glutathionylated yeast Grx2

	Oxidized ($yGrx2_{ox}$)	Glutathionylated ($yGrx2_{GS}$)
Diffraction data statistics		
Space group	$P4_12_12$	$P2_12_12_1$
Unit cell dimensions (Å)	$a=b=47.63$, $c=94.59$	$a=37.0076$, $b=45.2051$, $c=105.0348$
Resolution range (Å)	42.56–2.05 (2.16–2.05)	37.01–1.91 (2.01–1.91)
Measured reflections	90,136	247,826
Unique reflections	7295	14,326
Completeness (%)	99.8 (99.3)	99.7 (98.3)
Multiplicity (%)	12.3 (11.2)	8.6 (8.2)
R_{sym}	0.08 (0.294)	0.070 (0.389)
$\langle I/\sigma(I)\rangle$	28.9 (7.8)	23.6 (4.5)
Refinement statistics		
R_{factor}	0.198	0.196
R_{free}	0.230	0.262
No. of nonhydrogen atoms	899	1829
No. of water molecules	65	137
rmsd		
Bond lengths (Å)	0.012	0.012
Bond angles (Å)	1.450	1.392
Average *B*-factor (Å^2)		
Main chain	18.7	13.0
Side chain	22.2	16.9
Ramachandran analysis (%)		
Favored regions	97.9	95.8
Additionally allowed regions	2.1	4.2

The data for oxidized yGrx2 crystal were previously published and are shown here again for completeness.[34]

in a complex with GSH. Crystals of yGrx2-C30S with a glutathionyl mixed disulfide ($yGrx2_{GS}$) were obtained, and the structure was refined at 1.91 Å resolution (Table 4). However, again, we could not obtain crystals of reduced yGrx2-C30S after several trials.

$yGrx2_{ox}$ crystallizes in space group $P4_12_12$, with one molecule in the asymmetric unit, whereas glutathionylated yGrx2-C30S crystallizes in space group $P2_12_12_1$, with two molecules in the asymmetric unit (referred to as chains A and B). Structures were refined to final *R* values of *R*-factor = 0.198 and $R_{free}=0.230$ ($yGrx2_{ox}$) and *R*-factor = 0.196 and $R_{free}=0.262$ ($yGrx2_{GS}$). The high quality of the electron density maps allowed an accurate assignment of the entire polypeptide chain of $yGrx2_{ox}$ (109 residues). Chain A of $yGrx2_{GS}$ and residues 2 through 108 of $yGrx2_{GS}$ chain B were also assigned. Molecules of GSH were modeled as bound to each of the chains A and B in the $yGrx2_{GS}$ structure. Ramachandran analyses showed that 97.9% of the residues in the $yGrx2_{ox}$ and 95.8% of the residues in the $yGrx2_{GS}$ structures were in the most favored regions and that no residues were in disallowed regions.

The overall yGrx2 structure is similar to previously determined Grx structures with a central mixed four-stranded β-sheet flanked by five α-helices (Fig. 5). The active site is localized to the second α-helix and the loop that precedes it. The N-terminal active site cysteine, Cys27, is solvent exposed and the C-terminal Cys30 is buried one turn later along the helix α2 in the interior of the molecule. The distance between the γ-sulfur atoms of Cys27 and Cys30 in the intramolecular disulfide bond is 2.07 Å (Fig. 6a) and the distance between the γ-sulfur atoms of Cys27 and the glutathione cysteine (Cys_{GS}) in the mixed disulfide bond is 2.08 Å (Fig. 6b).

The $yGrx2_{ox}$ and $yGrx2_{GS}$ models have very similar tertiary structures (Fig. 5). The alignment of the $yGrx2_{ox}$ and $yGrx2_{GS}$ structures results in an overall rmsd of 0.59 Å for all 109 C^{α} atoms. Despite

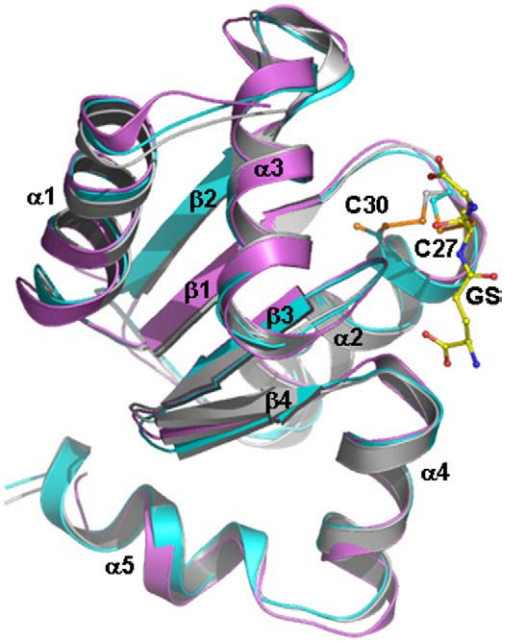

Fig. 5. Cartoon representation of the overall fold of yGrx1 and yGrx2 showing the structural alignment of $yGrx1_{GS}$ (α-carbon atoms in violet; PDB code 2JAC),[22] $yGrx2_{ox}$ (α-carbon atoms in gray) and $yGrx2_{GS}$ (α-carbon atoms in cyan). The GSH molecule bonded to the yGrx2-C30S mutant is shown in yellow.

the global similarity between $yGrx2_{ox}$ and $yGrx2_{GS}$, local conformational changes between structures of yGrx2 in the oxidized and glutathionylated forms occur in the active-site loop that is situated between the strand β1 and the helix α2. Several residues changed their conformation in the $yGrx2_{GS}$ structure, in comparison to the $yGrx2_{ox}$ structure, and interact with the GSH moiety (Fig. 7).

Both yGrx2 structures are very similar to those determined for yGrx1 in the reduced [Protein Data Bank (PDB) code 2JAD] and glutathionylated (PDB code 2JAC) forms (Fig. 5).[22] The alignment of $yGrx2_{GS}$ with $yGrx1_{GS}$ results in an rmsd of 0.7 Å for 108 C^{α} atoms of yGrx2, and the interactions between these proteins and the GSH moiety are very similar (see Supplementary Data). Other Grx structures have been determined with a glutathionyl mixed disulfide: human Grx1 (PDB code 1B4Q),[28] human Grx2 (PDB code 2FLS),[35] *E. coli* Grx1 (PDB code 1GRX)[9] and *E. coli* Grx3 (PDB code 3GRX).[11] Comparison of these structures shows that the Grx residues that interact with the GSH moiety are highly conserved (Fig. 2a and b). Nevertheless, there are differences among Grx enzymes and also between yGrx1 and yGrx2 (see below).

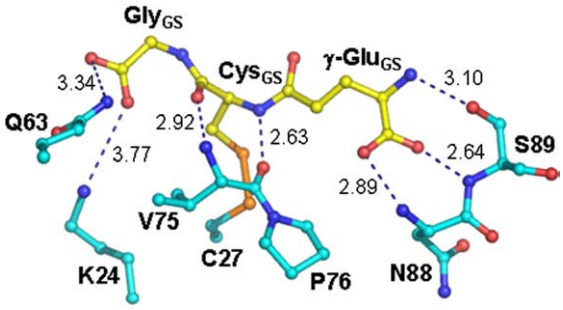

Fig. 7. yGrx2 interactions with GSH in the $yGrx2_{GS}$ structure. yGrx2 residues involved in interactions with the GSH moiety are represented in cyan and the GSH is shown in yellow. The hydrogen bonds and salt bridges are indicated by blue dashed lines, with the atomic distances in angstroms.

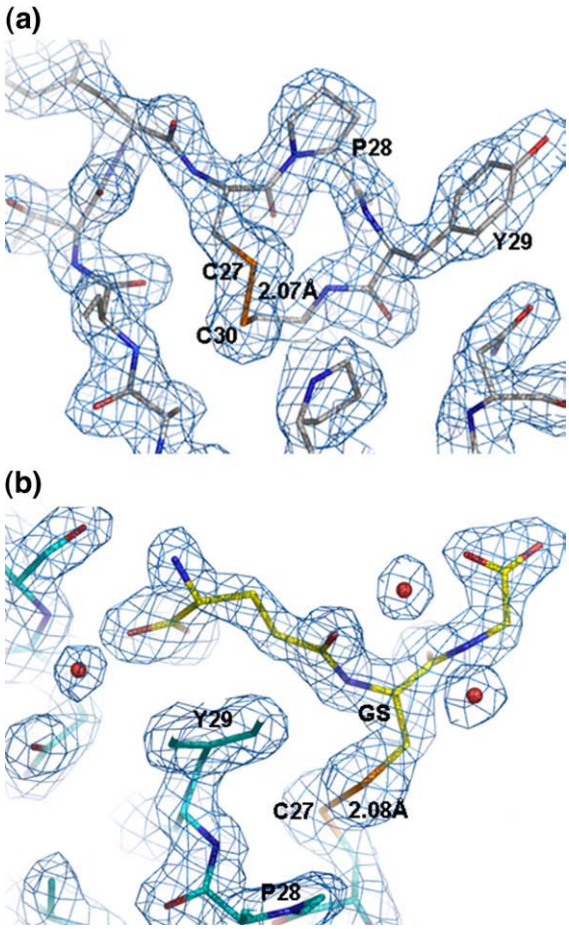

Fig. 6. Electron density maps ($2F_o - F_c$, contoured at 1.0σ) for the active site of (a) $yGrx2_{ox}$ and (b) $yGrx2_{GS}$. The continuous electron density between the sulfur atoms of Cys27 and Cys30 and Cys27 and the GSH cysteine residue show the disulfide bonds. The bond lengths of the intramolecular disulfide and the mixed disulfide with GSH are 2.07 and 2.08 Å, respectively.

The alignment of the $yGrx2_{GS}$ structure with the glutathionylated structures of human Grx1, human Grx2, *E. coli* Grx1 and *E. coli* Grx3 resulted in an overall rmsd of 1.67 Å (for 99 C^{α} atoms of yGrx2), 1.20 Å (for 97 C^{α} atoms of yGrx2), 2.08 Å (for 64 C^{α} atoms of yGrx2) and 1.68 Å (for 79 C^{α} atoms of yGrx2), respectively. Therefore, the overall structure of yGrx2 is more similar to the yGrx1 and human Grx1 and Grx2 structures than to the bacterial counterparts. These eukaryotic Grx structures have the same secondary structural elements, whereas *E. coli* Grx structures do not possess the first helix found in the eukaryotic Grxs, and *E. coli* Grx1 does not possess the last helix found in the other Grxs.

Comparison between yGrx2 and yGrx1 structures

Although the overall structures of yGrx1 and yGrx2 are very similar, an evident difference between the $yGrx2_{GS}$ and $yGrx1_{GS}$ structures is the conformation adopted by Ser30. In $yGrx1_{GS}$, the Ser30 side chain is directed toward Cys27, whereas in $yGrx2_{GS}$ the Ser30 side chain is turned to the opposite side (Fig. 8). In fact, the distance between the Ser30 hydroxyl oxygen and the sulfur atom of Cys27 is 3.47 Å in $yGrx1_{GS}$ and 5.14 Å in $yGrx2_{GS}$. Assuming that a cysteine at position 30 could have a side-chain conformation similar to that of serine in the C30S mutants of both $yGrx1_{GS}$ and $yGrx2_{GS}$, Cys30 of $yGrx1_{GS}$ would be able to attack the Cys27 and form an intramolecular disulfide bond, whereas the Cys30 of $yGrx2_{GS}$ would be in an unfavorable configuration for an attack on the corresponding mixed disulfide between Cys27 and GSH. If the formation of the intramolecular disulfide bond is disfavored in yGrx2, reduction of the glutathionyl mixed disulfide by an external nucleophile, such as

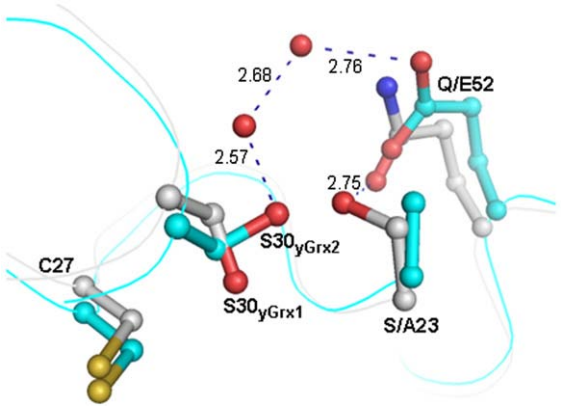

Fig. 8. Side-chain conformation of Ser30 in the structures of the C30S mutants of yGrx1[22] (gray) and yGrx2 (cyan) in their glutathionylated forms. It is clear that the distances from the Cys27 sulfur atoms (yellow) to the Ser30 oxygen atom (red) are very different between yGrx1 and yGrx2, indicating that the conformation of a Ser30 residue in yGrx2 is less favorable to attack the mixed disulfide.

GSH, is then favored (Fig. 1). Consequently, the monothiol mechanism (involved in the HED assay) is also favored.

Corroborating the above interpretation, in *E. coli* Grx3 glutathionylated structure,[11] Ser14 (which replaces the C-terminal active-site cysteine in this structure) presents a more buried conformation similar to that of $yGrx2_{GS}$ Ser30. In all other Grx structures reported in the glutathionylated form (all obtained with mutations of the C-terminal active-site cysteine to serine), including the *E. coli* Grx1,[9] the conformation of this Ser is similar to that found in $yGrx1_{GS}$. The more buried conformation of Ser30 in the $yGrx2_{GS}$ structure appears to be related to the interaction with the Glu52 carboxylate via two water molecules (Fig. 8). The distance between the oxygen of the carboxylate of Glu52 and the hydroxyl of Ser30 is 5.02 Å in $yGrx2_{GS}$. Similarly, *E. coli* Grx3 possesses the Glu30 residue, and an oxygen atom of its carboxylate group is located at 5.74 Å from the hydroxyl of Ser14 in its glutathionylated structure. Glu30 of *E. coli* Grx3 does not occupy the same position as yGrx2 Glu52, although the distances between the carboxylate groups of these Glu residues and the hydroxyl of the Ser are similar in both structures. Also, in both structures, the Ser adopts a more buried conformation than that adopted in other Grx glutathionylated structures. Remarkably, like yGrx2, *E. coli* Grx3 possesses higher monothiolic activity than *E. coli* Grx1, although to a much lower extent (twofold).

Other Grxs, such as pig Grx and human Grx1, possess an Asp residue at the equivalent position of yGrx2 Glu52. In these Grxs, however, there is an Ile residue that prevents the contact (direct or indirect) between the Asp and the C-terminal active-site residue. In the equivalent position of the mammalian Grx isoleucine residue, yGrx2 possesses an alanine residue (Ala23), which, due to the short side chain, does not prevent interaction between Ser30 and Glu52 (Fig. 8). *E coli* Grx3 also does not possess bulky residues that could prevent interactions between Ser14 and Glu30. Yeast Grx1 possesses a Gln52 replacing Glu52; however, this residue makes a hydrogen bond with the hydroxyl of Ser23 (yGrx2 Ala23) and does not interact with Ser30 (Fig. 8).

Our analyses suggest that the unfavorable conformation of yGrx2 Cys30 to form intramolecular disulfide could be related to interactions established with Glu52, which are possible due to the non-interfering side chain of Ala23. In contrast, the favorable conformation of yGrx1 Cys30 to attack the Grx-SG is probably related to the fact that those interactions present in yGrx2 are not possible in yGrx1 due to the substitution of Ala23 by Ser23, which forms a hydrogen bond with Gln52, avoiding the interaction between Cys30 and Gln52.

In order to test this hypothesis, we constructed mutants of both yGrx1 and yGrx2 (yGrx1-S23A, yGrx1-S23A-Q52E, yGrx2-A23S and yGrx2-A23S-E52Q). yGrx1-S23A and yGrx1-S23A-Q52E presented specific activities 3.4- and 3.0-fold higher than that of the wild-type yGrx1, respectively, whereas yGrx2-A23S and yGrx2-A23S-E52Q mutants exhibited specific activities 1.7- and 2.3-fold lower than that of the wild-type yGrx2, respectively (Table 1).

The higher activity of yGrx1-S23A and the lower activity of yGrx2-A23S compared with the activities of their respective wild-type isoforms indicated that these residues are in fact involved in the variation in the activities between dithiolic yGrxs. To further corroborate our hypothesis, the yGrx1 and yGrx2 double mutants should have higher and lower specific activities, respectively, than the single mutants yGrx1-S23A and yGrx2-A23S, indicating that the residues Ser/Ala23 and Gln/Glu52 have an additive effect in the activity of dithiolic yGrxs. However, this additive effect of Ser/Ala23 and Gln/Glu52 can be observed only in the yGrx2-A23S-Q52E double mutant, but not in yGrx1-S23A-E52Q (Table 1). Consequently, it is not clear if Gln/Glu52 is really related with the variation in the specific activity of dithiolic yGrxs.

Another possibility is that only Ser/Ala23 but not Gln/Glu52 exerts influence on yGrx1 and yGrx2 activities. In this case, Ser23 in yGrx1 could act as a base, taking away the proton from Cys30, favoring thiolate formation and, consequently, the attack of Cys30 on the Grx-SG intermediate (Fig. 1, reaction c). As a result, the formation of the intramolecular disulfide bond would switch the mechanism from the monothiol to the dithiol, which would result in a lower reaction rate in the HED assay, as discussed before. In the case of yGrx2, the more inert character of Ala23 should not influence the reactivity of Cys30 in the Grx-SG intermediate, allowing the reduction of the mixed disulfide by an external GSH molecule, therefore favoring the monothiol mechanism. This feature is consistent with the observation that yGrx1 presented higher K_M for GSH and lower k_{cat} values compared to yGrx2. This hypothesis is also in agreement with the mutagenesis experiments, since the

substitution of Ala23 by Ser in yGrx2-A23S mutant provokes a decrease in its specific activity compared with the yGrx2 wild-type enzyme, whereas the substitution of Ser23 by Ala in yGrx1-S23A causes an increase in its specific activity compared with the yGrx1 (Table 1).

It is important to mention here that in the structure of $yGrx1_{GS}$ the N-terminal active-site Cys27 residue is not bonded to the cysteine of GSH,[22] whereas in the $yGrx2_{GS}$ structure the glutathionyl mixed disulfide is observed (Fig. 6b). This difference might be a complicating factor for the comparison of these two structures, because it could have relevant consequences with respect to local structural conformations. However, as mentioned by the authors, the disulfide bond of yGrx1-SG was probably broken upon exposure to synchrotron radiation, and the orientation of GSH and yGrx1 residues probably was not affected, since the interactions with the GSH moiety were similar to those found in other glutathionylated Grx structures.[22,28,35] Furthermore, there are structures available in the PDB where the glutathionyl mixed disulfide is present and the serine residues equivalent to yGrx1 Ser30 presented the same conformation as in the $yGrx1_{GS}$ structure.[9,28] Additionally, the hypotheses raised here from structural comparisons were strengthened by biochemical assays with mutant proteins (Table 1).

Another aspect that is probably related to the different biochemical activities of yGrx1 and yGrx2 is their redox potential. In fact, Grx1 and Grx3 from *E. coli* also share high amino acid sequence and overall structure similarity, although they possess very distinct redox potentials ($\Delta E^{\circ\prime} = 35$ mV).[36] In contrast, Grx1 and Grx2 from humans possess more similar redox potentials ($\Delta E^{\circ\prime} = 11$ mV),[37] although they do not share the same degree of similarity. In this case, it is important to mention that human Grx2 presents several unusual features such as an additional disulfide bond with a very negative redox potential (−317 mV).[36] Several aspects of the relationships between redox potential and protein structure remain to be established.

In conclusion, the great enzymatic difference observed between yGrx1 and yGrx2 appears not to be related to the pK_a of their reactive cysteines, but to specific structural features of these enzymes. Considering the conformation of Ser30/Cys30 in dithiolic yGrxs glutathionylated structures and the influence of Ser23 and Ala23 in the yGrx1 and yGrx2 activities, respectively, we hypothesize that yGrx2 could be more specially adapted than yGrx1 to the monothiol mechanism. These structural and functional differences between yGrx1 and yGrx2 might reflect variations in substrate specificity.

Materials and Methods

Cloning, expression and purification

Wild-type yeast *GRX2* gene was cloned into the pET15b expression vector, expressed in *E. coli* and purified by cobalt-affinity chromatography as previously described.[34]

Site-directed mutagenesis was employed to mutate the cysteine 30 residue of Grx2 to a serine residue. The *GRX1* and *GRX2* genes were PCR amplified from *S. cerevisiae* genomic DNA of the strain W303 with the primers 5′-CGCGATCCATATGATGGTATCTCAAGAAAC-3′ (forward *GRX1*), 5′-CGCAAGCTTGGATCCTTAATTTGCAAGAATAGG-3′ (reverse *GRX1*), 5′-CGCGATCCATATGATGGTATCCCAGGAAACAGTTGCTCACGTAAAGGATCTGATTGGCCAAAAGGAAGTGTTTGTTGCAGCAAAGACATACTGCCCTTACAGCAAAGCTACTTTG-3′ (forward *GRX2-C30S*, mutated sequence underlined), 5′-CGCAAGCTTGGATCCCTATTGAAATACCGGCTTC-3′ (reverse *GRX2-C30S*). The forward primers contain NdeI restriction sites and the reverse primers contain BamHI restriction sites. The PCR products and the expression vector pET15b were first digested with NdeI and BamHI, and then the products were ligated into the pET15b. The *GRX1-S23A*, *GRX1-C30S* and *GRX2-A23S* mutants were prepared with the QuickChange Site-Directed Mutagenesis Kit from Stratagene according to the manufacturer's recommendations. The pET15b/*GRX1* and pET15b/*GRX2* plasmids were used as templates with two complementary primers containing the desired mutation (underlined): 5′-GAGATCTTCGTCGCAGCAAAAACGTACTGTCC-3′ (forward *GRX1-S23A*); 5′-CGTACTGTCCATACTCTCATGCAGCCCTAAAC-3′ (forward *GRX1-C30S*); 5′-GAAGTGTTTGTTGCATCCAAGACATACTGCCC-3′ (forward *GRX2-A23S*). The mutants *GRX1-S23A-Q52E* and *GRX2-A23S-E52Q* were also prepared using the same strategy, with the pET15b/*GRX1-S23A* and the pET15b/*GRX2-A23S* plasmids as templates and the following primers: 5′-GTT CTG GTT TTG GAG TTG AAT GAC ATG AAG-3′ (forward *GRX1-Q52E*); 5′-G GCC CTT GTG TTG CAG TTA GAT GAA ATG AGC-3′ (forward *GRX2-E52Q*). The gene sequences were confirmed by automated DNA sequencing and the resulting plasmids were used to transform *E. coli* BL21(DE3). Protein expression was induced by the addition of 1 mM IPTG to cultures grown in LB medium at 310 K to $OD_{600} = 0.8$. The cells were harvested after 3 h of incubation at 310 K.

Cell pellets were resuspended in 20 mM sodium phosphate buffer, pH 7.4, 500 mM NaCl, 20 mM imidazole and 1 mM PMSF and lysed by sonication. Subsequently, the cell extract was kept on ice for 20 min during a 1% streptomycin sulfate treatment. The extract was centrifuged at 16,000*g* for 45 min to remove cell debris, and the supernatant was further clarified by filtration. The proteins were purified by metal-affinity chromatography (Nickel-Hi-trap from GE Healthcare or Cobalt-Talon metal-affinity resin from Clontech) with imidazole gradients. Protein purity was confirmed by SDS-PAGE.

Yeast Grx1 and Grx2 his-tag fusion proteins were digested with the Thrombin Clean Cleave Kit by Sigma, following the manufacturer's protocol.

Assay for Grx activity

Specific activities of yGrx1, yGrx2 and of the mutants yGrx1-S23A, yGrx1-C30S, yGrx1-S23A-Q52E, yGrx2-A23S, yGrx2-C30S and yGrx2-A23S-E52Q were measured with the standard assay for Grxs, at 30 °C, using a mixed disulfide between HED and GSH as the substrate.[23] Concentrations of yGrx1, yGrx2 and yGrx2-C30S were varied from 50 to 400, 5 to 35 and 10 to 200 nM, respectively, and the concentrations of the mutants yGrx1-S23A, yGrx1-S23A-Q52E, yGrx1-C30S, yGrx2-A23S and yGrx2-A23S-

E52Q were varied from 10 to 100 nM. The reaction mixture, containing 100 mM Tris–HCl, pH 7.4, 6 μg/ml GR, 1 mM GSH, 0.7 mM HED, 0.1 mg/ml bovine serum albumin (BSA), 0.2 mM NADPH and 2 mM ethylenediaminetetraacetic acid (EDTA) in a volume of 1 ml, was incubated at 30 °C for 3 min for the formation of the mixed disulfide between GSH and HED. The reaction was started by the addition of Grx and followed by the decrease in the absorbance at 340 nm due to the oxidation of NADPH. Measured activities in all assays were corrected by subtracting the velocities of the control reactions without the enzyme, and three independent experiments were performed at each substrate concentration.

Two-substrate kinetics

Two-substrate kinetics were performed at 30 °C, varying the concentration of HED from 0.03 to 2.2 mM at fixed concentrations of GSH (0.5, 1.0, 1.5 and 2.0 for yGrx1; 0.5, 1.0 and 1.5 for yGrx2).[21] The reaction mixture contained the same components at the same concentrations as described for the measurement of Grx-specific activities. In this case, we also waited for 3 min for the formation of the mixed disulfide between GSH and HED before starting the reaction with the addition of Grx. The concentrations of yGrx1 and yGrx2 used in these assays were 500 and 50 nM, respectively. Measured activities in all assays were corrected by subtracting the velocities of the control reactions without the enzyme. Three independent experiments were performed at each substrate concentration, and the apparent K_M and V_{max} values were determined by non-linear regression of Michaelis–Menten plots. The reciprocal values of V_{max}^{app} were plotted *versus* the reciprocal of the GSH concentration to provide the kinetic parameters for GSH.[27]

pK_a determination of N-terminal cysteine

To determine the pK_a of the N-terminal active-site cysteine of yGrx1, yGrx2 and the yGrx2-C30S mutant, the prereduced enzymes were incubated at different pH values with or without 300 μM iodoacetamide for 3 min at room temperature.[12,14,26] After incubation, a 100-fold dilution in an ice-cold bath quenched the reaction mixture, and the protein was assayed for activity with the standard assay for Grx, described in Materials and Methods. The percentage of remaining activity at each pH was determined by comparing the activity of the enzyme incubated with and without iodoacetamide at the same pH. The concentration of enzyme used in the assays was 250, 20 and 100 nM for yGrx1, yGrx2 and yGrx2-C30S, respectively. Buffers for incubation of enzymes were used at 10 mM concentration (KCl–HCl, pH 1.0 and 1.5; citrate–phosphate, pH 2.0, 2.5, 3.0, 3.5, 4.0, 5.0 and 6.0; Tris–HCl, pH 7.0 and 8.0), and for the assay, 100 mM Tris–HCl buffer, pH 7.4, was used. The ionic strength was adjusted to 0.5 M by the addition of NaCl.

In a second, independent approach, the pK_a of the N-terminal active-site cysteine residues was determined by monobromobimane alkylation that generates a fluorescent product (λ_{exc} 396 nm, λ_{em} 482 nm).[30] yGrx1 and yGrx2 were previously reduced by excess DTT (100 mM) for 2 h in the presence of 0.1 mM diethylenetriamine pentaacetic acid at room temperature. Excess DTT was removed by size-exclusion chromatography (PD-10 columns, GE Healthcare), with 5 mM Tris–HCl, pH 7.5 (Grx2) or pH 8.5 (Grx1), as elution buffer. Protein concentration was determined by absorbance at 280 nm and specific extinction coefficient ($\varepsilon_{yGrx1} = 6085$, $\varepsilon_{yGrx2} = 4470$). yGrx1 and yGrx2 (10 μM) were incubated with monobromobimane (2 μM) at various pH values in 96-well plates in triplicate. All buffers used in the alkylation reactions were at 50 mM concentration (KCl–HCl, pH 1.0 and 1.5; citrate–phosphate, pH 2.0 to 5.0) and reactions proceeded at 37 °C with shaking. The ionic strength was adjusted to 0.5 M by the addition of NaCl. The rates of monobromobimane alkylation were determined by extrapolation of the maximum inclination in the kinetics. As a control, it was verified that the fluorescence of the same protein–monobromobimane adduct does not change as a function of pH.

The plots displayed in Fig. 4a and b were fitted by non-linear regression to sigmoidal dose–response curves with GraphPad Prism4 software. The Hill slope utilized was equal to 1.00. The pK_a values were obtained from the inflection point, in this case, log EC_{50}.

Crystallization and X-ray data collection

In an attempt to obtain the crystal structure of yGrx2 in different oxidative states, prior to crystallization, yGrx2 samples (10 mg/ml in 5 mM Tris–HCl, pH 7.4) were submitted to treatment for 1 h at 310 K with 1 mM hydrogen peroxide, 10 mM *t*-BOOH, 3 mM diamide, 10 mM DTT or 10 mM GSH. We also subjected freshly grown yGrx2 crystals to soaking experiments with 10 mM DTT and 10 mM GSH in an effort to obtain the structure of reduced yGrx2. Furthermore, to obtain yGrx2-C30S with a glutathionyl mixed disulfide for crystallization, the purified protein was first incubated with 50 mM DTT for 1 h at room temperature. Excess DTT was removed by gel-filtration chromatography using a PD10 column (GE Healthcare). Then, the reduced protein was treated with 25 mM GSSG for 1 h at room temperature followed by gel-filtration chromatography. The glutathionylated sample of yGrx2-C30S was concentrated to 13 mg/ml in 5 mM Hepes, pH 7.4.

Crystallization trials for yGrx2 were performed with the hanging-drop vapor-diffusion method, as previously described.[34] Crystals of yGrx2 suitable for X-ray diffraction measurements were obtained under all the treatments in condition 10 of the Crystal Screen kit [30% polyethylene glycol (PEG) 4000, 0.1 M sodium acetate, pH 4.6, and 0.2 M ammonium acetate]. Crystals of yGrx2-C30S with a glutathionyl mixed disulfide were obtained in condition 22 of the Crystal Screen kit; after optimization, we obtained crystals suitable for X-ray diffraction experiments under the following conditions: 30% PEG 4000/0.1 M sodium acetate, pH 5.4/0.2 M sodium acetate.

Crystals were produced from samples subjected to all treatments described and different data sets were collected. The crystals, cryoprotected by 20% glycerol, were cooled to 110 K and X-ray diffraction data were collected using synchrotron radiation at the protein crystallography beamline D03B MX1 at the Brazilian Synchroton Light Laboratory.

Data processing, structure solution and refinement

All data sets were indexed and integrated with MOSFLM[38] and scaled and merged using SCALA[39,40] from the CCP4 suite.[41] The first structure of yGrx2 (oxidized with *t*-BOOH) was solved by molecular replacement with the program AMORE,[42] using as a search model a polyalanine theoretical model constructed with the program MODELLER[43] and the coordinates of a thioltransferase from *Sus scrofa* (PDB code 1KTE),[44] as previously described.[34] The other structures of yGrx2 and

glutathionylated yGrx2-C30S were solved by molecular replacement with the refined structure of oxidized yGrx2 ($yGrx2_{ox}$) using the programs AMORE and PHASER.[42,45]

Refinements of all yGrx2 structures were performed with REFMAC 5.0,[46] and a TLS atomic displacement model[47] was used in the later stages of the structure refinement of yGrx2-C30S with a glutathionyl mixed disulfide. The programs O[48] and COOT[49] were used for visual inspection and manual model building between the refinement cycles. The stereochemical quality of the final models was assessed by PROCHECK.[50] Structural alignments were performed with the programs O[48] or COOT.[49] Molecular graphics figures were generated with the program PyMOL.[51]

Protein Data Bank accession numbers

Atomic coordinates of the *S. cerevisiae* Grx2 oxidized and glutathionylated structures have been deposited in the RCSB PDB with the accession codes 3D4M and 3D5J, respectively.

Acknowledgements

This work was supported by grants from the Fundação de Amparo à Pesquisa do Estado de São Paulo, by the Conselho Nacional de Desenvolvimento Científico e Tecnológico (Projeto Milenio Redoxoma), the Brazilian Synchrotron Light Laboratory under proposal D03B-1795 and by Spanish MCyT, grant BFU2006-02990 (BMC). We thank Dr. Gerardo Ferrer-Sueta (Universidad de la Republica, Montevideo, Uruguay) and Dr. Marilene Demasi (Instituto Butantan, São Paulo, Brazil) for helpful discussions and experimental support.

Supplementary Data

Supplementary data associated with this article can be found, in the online version, at doi:10.1016/j.jmb.2008.10.055

References

1. Holmgren, A. (1989). Thioredoxin and glutaredoxin systems. *J. Biol. Chem.* **264**, 13963–13966.
2. Holmgren, A. (1976). Hydrogen donor system for *Escherichia coli* ribonucleoside–diphosphate reductase dependent upon glutathione. *Proc. Natl Acad. Sci. USA*, **73**, 2275–2279.
3. Holmgren, A. (1978). Glutathione-dependent enzyme reactions of the phage T4 ribonucleotide reductase system. *J. Biol. Chem.* **253**, 7424–7430.
4. Holmgren, A. (1979). Glutathione-dependent synthesis of deoxyribonucleotides. Characterization of the enzymatic mechanism of *Escherichia coli* glutaredoxin. *J. Biol. Chem.* **254**, 3672–3678.
5. Bushweller, J. H., Åslund, F., Wüthrich, K. & Holmgren, A. (1992). Structural and functional characterization of the mutant *Escherichia coli* glutaredoxin (C14→S) and its mixed disulfide with glutathione. *Biochemistry*, **31**, 9288–9293.
6. Lillig, C. H., Berndt, C. & Holmgren, A. (2008). Glutaredoxin systems. *Biochim. Biophys. Acta*, **1780**, 1304–1317.
7. Gallogly, M. M. & Mieyal, J. J. (2007). Mechanisms of reversible protein glutathionylation in redox signaling and oxidative stress. *Curr. Opin. Pharmacol.* **7**, 381–391.
8. Srinivasan, U., Mieyal, P. A. & Mieyal, J. J. (1997). pH profiles indicative of rate-limiting nucleophilic displacement in thioltransferase catalysis. *Biochemistry*, **36**, 3199–3206.
9. Bushweller, J. H., Billeter, M., Holmgren, A. & Wüthrich, K. (1994). The nuclear magnetic resonance solution structure of the mixed disulfide between *Escherichia coli* glutaredoxin (C14→S) and glutathione. *J. Mol. Biol.* **235**, 1585–1597.
10. Fernandes, A. P. & Holmgren, A. (2004). Glutaredoxins: glutathione-dependent redox enzymes with functions far beyond a simple thioredoxin backup system. *Antioxid. Redox Signal.* **6**, 63–74.
11. Nordstrand, K., Åslund, F., Holmgren, A., Otting, G. & Berndt, K. D. (1999). NMR structure of *Escherichia coli* glutaredoxin 3–glutathione mixed disulfide complex: implications for the enzymatic mechanism. *J. Mol. Biol.* **286**, 541–552.
12. Jao, S., Ospina, S. M. E., Berdis, A. J., Starke, D. W., Post, C. B. & Mieyal, J. J. (2006). Computational and mutational analysis of human glutaredoxin (thioltransferase): probing the molecular basis of the low pK_a of cysteine 22 and its role in catalysis. *Biochemistry*, **45**, 4785–4796.
13. Yang, Y. & Wells, W. W. (1991). Identification and characterization of the functional amino acids at the active center of pig liver thioltransferase by site-directed mutagenesis. *J. Biol. Chem.* **266**, 12759–12765.
14. Gan, Z., Sardana, M. K., Jacobs, J. W. & Polokoff, M. A. (1990). Yeast thioltransferase—active site cysteines display differential reactivity. *Arch. Biochem. Biophys.* **282**, 110–115.
15. Luikenhuis, S., Perrone, G., Dawes, I. W. & Grant, C. M. (1998). The yeast *Saccharomyces cerevisiae* contains two glutaredoxin genes that are required for protection against reactive oxygen species. *Mol. Biol. Cell*, **9**, 1081–1091.
16. Pedrajas, J. R., Porras, P., Martínez-Galisteo, E., Padilla, C. A., Miranda-Vizuete, A. & Bárcena, J. A. (2002). Two isoforms of *Saccharomyces cerevisiae* glutaredoxin 2 are expressed *in vivo* and localize to different subcellular compartments. *Biochem. J.* **364**, 617–623.
17. Porras, P., Padilla, C. A., Krayl, M., Voos, W. & Barcena, J. A. (2006). One single in-frame AUG codon is responsible for a diversity of subcellular localizations of glutaredoxin 2 in *Saccharomyces cerevisiae*. *J. Biol. Chem.* **281**, 16551–16562.
18. Rodríguez-Manzaneque, M. T., Ros, J., Cabiscol, E., Sorribas, A. & Herrero, E. (1999). Grx5 glutaredoxin plays a central role in protection against protein oxidative damage in *Saccharomyces cerevisiae*. *Mol. Cell. Biol.* **19**, 8180–8190.
19. Ojeda, L., Keller, G., Muhlenhoff, U., Rutherford, J. C., Lill, L. & Winge, D. R. (2006). Role of glutaredoxin 3 and glutaredoxin 4 in the iron regulation of Aft1 transcriptional activator in *Saccharomyces cerevisiae*. *J. Biol. Chem.* **281**, 17661–17669.
20. Rodríguez-Manzaneque, M. T., Tamarati, J., Belli, G., Ros, J. & Herrero, E. (2002). Grx5 is a mitochondrial glutaredoxin required for the activity of iron/sulfur enzymes. *Mol. Biol. Cell*, **13**, 1109–1121.

21. Mesecke, N., Mittler, S., Eckers, E., Herrmann, J. M. & Deponte, M. (2008). Two novel monothiol glutaredoxins from *Saccharomyces cerevisiae* provide further insight into iron–sulfur cluster binding, oligomerization, and enzymatic activity of glutaredoxins. *Biochemistry*, **47**, 1452–1463.
22. Håkansson, K. O. & Winther, J. R. (2007). Structure of glutaredoxin Grx1p C30S mutant from yeast. *Acta Crystallog., Sect. D: Biol. Crystallogr.* **63**, 288–294.
23. Holmgren, A. & Åslund, F. (1995). Glutaredoxin. *Methods Enzymol.* **252**, 283–292.
24. Chenna, R., Sugawara, H., Koile, T., Lopez, R., Gibson, T. J., Higgins, D. G. & Thompson, J. D. (2003). Multiple sequence alignment with the Clustal series of programs. *Nucleic Acids Res.* **31**, 3497–3500.
25. Clamp, M., Cuff, J., Searle, S. M. & Barton, G. J. (2004). The Jalview Java alignment editor. *Bioinformatics*, **20**, 426–427.
26. Mieyal, J. J., Starke, D. W., Gravina, S. A. & Hocevar, B. (1991). Thioltransferase in human red blood cells: kinetics and equilibrium. *Biochemistry*, **30**, 8883–8891.
27. Segel, H. I. (1975). Enzyme Kinetics: Behavior and Analysis of Rapid Equilibrium and Steady-State Enzyme Systems. Wiley, New York.
28. Yang, Y., Jao, S., Nanduri, S., Starke, D. W., Mieyal, J. J. & Qin, J. (1998). Reactivity of the human thioltransferase (glutaredoxin) C7S, C25S, C78S, C82S mutant and NMR solution structure of its glutathionyl mixed disulfide intermediate reflect catalytic specificity. *Biochemistry*, **37**, 17145–17156.
29. Johansson, C., Lillig, C. H. & Holmgren, A. (2004). Human mitochondrial glutaredoxin reduces *S*-glutathionylated proteins with high affinity accepting electrons from either glutathione or thioredoxin reductase. *J. Biol. Chem.* **279**, 7537–7543.
30. Kosower, N. S., Kosower, E. M., Newton, G. L. & Ranney, H. M. (1979). Bimane fluorescent labels: labeling of normal human red cells under physiological conditions. *Proc. Natl Acad. Sci. USA*, **76**, 3382–3386.
31. Gilbert, H. F. (1990). Molecular and cellular aspects of thiol–disulfide exchange. *Adv. Enzymol. Relat. Areas Mol. Biol.* **63**, 69–172.
32. Szajewski, R. P. & Whitesides, G. M. (1980). Rate constants and equilibrium constants for thiol–disulfide interchange reactions involving oxidized glutathione. *J. Am. Chem. Soc.* **102**, 2011–2026.
33. Creighton, T. E. & Darby, N. J. (1993). Dissecting the disulfide couple folding pathway of bovine pancreatic inhibitor: forming the first disulfide bonds in analogues of the reduced protein. *J. Mol. Biol.* **232**, 873–896.
34. Johansson, C., Kavanagh, K. L., Gileadi, O. & Oppermann, U. (2007). Reversible sequestration of active site cysteines in a 2Fe2S-bridge dimmer provides a mechanism for glutaredoxin 2 regulation in human mitochondria. *J. Biol. Chem.* **282**, 3077–3082.
35. Åslund, F., Berndt, K. D. & Homlgren, A. (1997). Redox potentials of glutaredoxins and other thiol–disulfide oxidoreductases of the thioredoxin superfamily determined by direct protein–protein equilibria. *J. Biol. Chem.* **272**, 30780–30786.
36. Sagemark, J., Elgán, T. H., Bürglin, T. R., Johansson, C., Holmgren, A. & Berndt, K. D. (2007). Redox properties and evolution of human glutaredoxins. *Prot. Struct. Funct. Bioinf.* **68**, 879–892.
37. Discola, K. F., Oliveira, M. A., Monteiro, G. S., Bárcena, J. A., Porras, P., Padilla, A. *et al.* (2005). Crystallization and preliminary X-ray crystallographic studies of glutaredoxin 2 from *Saccharomyces cerevisiae* in different oxidation states. *Acta Crystallogr., Sect. F*, **61**, 445–447.
38. Leslie, A. G. W. (1992). Joint CCP4/ESF-EAMBCB. Newsletter Protein Crystallography 26. Daresbury Laboratory, Warrington, UK.
39. Kabush, W. (1988). Evaluation of single-crystal X-ray diffraction data from a position-sensitive detector. *J. Appl. Crystallogr.* **21**, 916–924.
40. Blessing, R. H. (1995). An empirical correction for absorption anisotropy. *Acta Crystallogr., Sect. A: Found. Crystallogr.* **51**, 33–38.
41. Collaborative Computational Project, Number 4. (1994). *Acta Crystallogr., Sect. D: Biol. Crystallogr.* **50**, 760–763.
42. Navaza, J. (1994). AmoRe: an automated package for molecular replacement. *Acta Crystallogr., Sect. D: Biol. Crystallogr.* **57**, 1367–1372.
43. Claude, J. B., Suhre, K., Notredame, C., Claverie, J. M. & Abergel, C. (2004). CaspR: a Web server for automated molecular replacement using homology modelling. *Nucleic Acids Res.* **32**, W606–W609.
44. Katti, S. K., Robbins, A. H., Yang, Y. & Wells, W. W. (1995). Crystal structure of thioltransferase at 2.2 Å resolution. *Protein Sci.* **4**, 1998–2005.
45. Read, R. J. (2001). Pushing the boundaries of molecular replacement with maximum likelihood. *Acta Crystallogr., Sect. D: Biol. Crystallogr.* **57**, 1373–1382.
46. Murshudov, G. N., Vagin, A. A. & Dodson, E. J. (1997). Refinement of macromolecular structures by the maximum-likelihood method. *Acta Crystallogr., Sect. D: Biol. Crystallogr.* **53**, 240–255.
47. Winn, M. D., Isupov, M. N. & Murshudov, G. N. (2001). Use of TLS parameters to model anisotropic displacements in macromolecular refinement. *Acta Crystallogr., Sect. D: Biol. Crystallogr.* **57**, 122–133.
48. Jones, T., Zou, J., Cowan, S. & Kjeldgaard, M. (1991). Improved methods for binding protein models in electron density maps and the location of errors in these models. *Acta Crystallogr., Sect. A: Found Crystallogr.* **47**, 110–119.
49. Emsley, P. & Cowtan, K. (2004). Coot: model-building tools for molecular graphics. *Acta Crystallogr., Sect. D: Biol. Crystallogr.* **60**, 2126–2132.
50. Laskowski, R. A., MacArthur, M. W., Moss, D. S. & Thornton, J. M. (1993). PHOCHECK: a program to check the stereochemical quality of protein structures. *J. Appl. Crystallogr.* **26**, 283–291.
51. DeLano, W. L. (2002). *The PyMOL Molecular Graphics System*. DeLano Scientific, San Carlos, CA.